

## The atomic structure of bakerite and its relationship to datolite

N. PERCHIAZZI,<sup>1,\*</sup> A.F. GUALTIERI,<sup>2</sup> S. MERLINO,<sup>1</sup> AND A.R. KAMPF<sup>3</sup>

<sup>1</sup>Dipartimento di Scienze della Terra, Università di Pisa, Via S. Maria 53, 56126 Pisa, Italy

<sup>2</sup>Dipartimento di Scienze della Terra, Università di Modena e Reggio Emilia, Via S. Eufemia 19, 41100 Modena, Italy

<sup>3</sup>Natural History Museum of Los Angeles County, 900 Exposition Blvd., Los Angeles, California 90007, U.S.A.

### ABSTRACT

Four samples of bakerite,  $\text{Ca}_4\text{B}_5\text{Si}_3\text{O}_{15}(\text{OH})_5$ , were studied by means of IR, TG/DSC, EPMA, and X-ray and neutron diffraction. Chemical analyses can readily discriminate bakerite from datolite,  $\text{Ca}_4\text{B}_4\text{Si}_4\text{O}_{16}(\text{OH})_4$ , by the distinctly lower  $\text{SiO}_2$  content of the former. The Rietveld refinement of the combined neutron and X-ray powder data allow the determination of the crystal structure of bakerite to  $R_p$  3.09%. The crystal structure can be derived from that of datolite by the substitution  $0.25\text{Si}^{4+} + 0.25\text{O}^{2-} \leftrightarrow 0.25\text{B}^{3+} + 0.25(\text{OH})^-$  at the Si-centered tetrahedral site. This leads to the crystal chemical formula  $\text{Ca}_4\text{B}_5\text{Si}_3\text{O}_{15}(\text{OH})_5$ . Both of the two hydrogen positions in the bakerite structure, one with full occupancy, the other with 25% occupancy, were precisely located. The water molecule generally thought to be present in bakerite structure is actually absent. The excess water detected in chemical analyses can be attributed to the presence of minor impurities. Given the consistent composition of bakerite from various localities and no evidence for substitution of B for Si in datolite, bakerite is retained as a distinct species. A possible explanation of the peculiar 5:3 boron to silicon ratio in bakerite is provided.

### INTRODUCTION

The mineral bakerite is generally considered to be a member of the gadolinite group with chemical composition  $\text{Ca}_x\text{B}_y(\text{BO}_4)_z(\text{SiO}_4)_3(\text{OH})_3 \cdot \text{H}_2\text{O}$ . Other members of the gadolinite group are gadolinite, homilite, minasgeraisite, datolite, and hingannite. These minerals provide important insights into petrogenetic processes and especially magmatic and hydrothermal crystallization. The chemical differences among the gadolinite minerals reflect different parental magma compositions and differences in crystallization processes. Thus, they can be used as geothermometers and paragenetic indicators.

Bakerite was first described by Giles (1903), with chemical formula  $\text{Ca}_8\text{B}_{10}\text{Si}_6\text{O}_{30}(\text{OH})_{10} \cdot \text{H}_2\text{O}$ , as white fine-grained nodules and veins occurring in altered volcanic rocks. According to Pemberton (1971), the true locality of Giles' material is Corkscrew Canyon, Death Valley, Inyo County, California. Other reported California occurrences of bakerite are at the nearby DeBely Wash (Kramer and Allen 1956) in microcrystalline masses, and at Sterling Borax mine, in tiny crystals (Murdoch 1962). The latter is the only reported occurrence of bakerite as single well-formed crystals and it was with this material that Murdoch (1962) determined the space group and cell for the species,  $P2_1/c$ ,  $a$  4.83,  $b$  7.60,  $c$  9.60 Å,  $\beta$  90°2',  $Z = 1$ . Several other bakerite occurrences are known, always as microcrystalline material: in diabase spilites from drill cores at Golcuk plateau, Sivas, Turkey (Baysal and Dilekoz 1975); in a diopside-bearing marble at Tory Hill, Ontario, Canada (Sabina 1978); in slag heaps at Casarza Ligure, Liguria, Italy (Palenzona 1985); and in gehlenite-spurrite-bearing skarns at Fuka, Okayama prefecture, Japan (Kusachi et al. 1994).

Palache et al. (1951) first pointed out the resemblance of the

X-ray powder patterns of bakerite and datolite, indicating their structural relationship, and on this assumption suggested for bakerite the chemical formula  $\text{Ca}_8\text{B}_{10}\text{Si}_6\text{O}_{30}(\text{OH})_{10}$  recalculated on the basis of  $\text{O} = 40$ . Considering that the bakerite formula given by Giles (1903) was calculated on the basis of  $\text{O} = 41$ , the only difference between the two proposed formulas is the water content, i.e., the possible presence of an additional water molecule in bakerite with respect to datolite.

Although the gadolinite group minerals are well known and well characterized, the structure of bakerite has never been determined. We undertook the present study to ascertain the true nature of bakerite and especially its relationship with datolite.

### MATERIALS AND METHODS

The samples investigated were (1) bakerite crystals from the Sterling Borax mine, Tick Canyon, Los Angeles County, California, U.S.A.; depository Natural History Museum of Los Angeles County, catalog number 45837 (micromount collection of L. Lobsenz, donated in 1999). (2) Bakerite crystals from the Sterling Borax mine, Tick Canyon, Los Angeles County, California, U.S.A.; from the research material of J.P. Murdoch (MS1531D) stored at the University of California, Los Angeles. Murdoch's single-crystal mounts for X-ray work accompany this material and make it clear that it corresponds to that reported in Murdoch (1962). (3) Bakerite type material, a microcrystalline marble-like mass from Corkscrew Canyon, Death Valley, Inyo County, California, U.S.A.; depository Harvard Mineralogical Museum, catalog number 92735. (4) Microcrystalline masses of bakerite from Corkscrew Canyon, Death Valley, Inyo County, California, U.S.A.; depository Natural History Museum of Los Angeles County, catalog number 14088. (5) Datolite from Rossena, Reggio Emilia, Italy; depository Museo di Storia Naturale dell'Università di Pisa, catalog number 4981.

A crystal from specimen no. 45837 matching the description in Murdoch (1962) was used to collect the single-crystal X-ray structure data. The crystal structure refinement was performed using the starting coordinates from the datolite structure (Foit et al. 1973). Information pertinent to this structural refinement is provided in Table 1.

X-ray powder patterns were collected from microcrystalline samples no. 92735 and no. 14088 with a Philips PW1050 automated diffractometer, using graphite monochromatized  $\text{CuK}\alpha$  radiation. Scans were recorded in the range 4 to 90° 2 $\theta$  with 0.02° steps and 46 s counting time. The patterns of the two samples nicely matched the JCPDS

\* E-mail: natale@dst.unipi.it

**TABLE 1.** Single-crystal data collection and structure refinement details for datolite (bakerite no. 45837)

Diffractometer	Bruker SMART Platform CCD
X-ray radiation/power	MoK $\alpha$ ( $\lambda = 0.71073 \text{ \AA}$ ) / 50 kV, 45 mA
Temperature	298(2) K
Crystal system, space group	Monoclinic, $P2_1/c$
Unit-cell dimensions	$a = 4.850(2) \text{ \AA}$ $b = 7.627(4) \text{ \AA}$ $c = 9.659(5) \text{ \AA}$ $\beta = 90.255(8)^\circ$
Volume	$357.3(3) \text{ \AA}^3$
Z, Calculated density	1, 2.899 g/cm $^3$
Absorption coefficient	$1.897 \text{ mm}^{-1}$
$F(000)$	312
Crystal size	$0.14 \times 0.13 \times 0.03 \text{ mm}$
Frame number/width/time	1255/0.3 $^\circ$ in $\omega$ /30 s
$\theta$ range	$3.40$ to $28.26^\circ$
Index ranges	$-6 \leq h \leq 4$ , $-10 \leq k \leq 8$ , $-11 \leq l \leq 12$
Reflections collected	1766
Independent reflections	732 ( $R_{\text{int}}^* = 0.0250$ )
Reflections, $F_o > 4\sigma(F_o)$	599
Completeness to $\theta = 28.29^\circ$	82.3%
Refinement method	Full-matrix least-squares on $F^2$
Parameters refined	77
Goof†	0.819
R indices [ $F_o > 4\sigma(F_o)$ ]	$R(F) \ddagger = 3.2\%$ , $wR(F)^2 \S = 9.7\%$
R indices (all data)	$R(F) \ddagger = 4.0\%$ , $wR(F)^2 \S = 10.3\%$
Largest diff. peak / hole	$+0.56 / -0.51 \text{ e/\AA}^3$
Notes: $w = 1 / [\sigma^2(F_o^2) + (aP)^2 + bP]$ where $P = [2F_o^2 + \text{Max}(F_o^2, 0)] / 3$ .	
* $R_{\text{int}} = \sum  F_o^2 - F_o^2(\text{mean})  / \sum F_o^2$ .	
† $\text{Goof} = S = \{\sum [w(F_o^2 - F_c^2)]^2 / (n-p)\}^{1/2}$ .	
‡ $R(F) = \sum  F_o - F_c  / \sum F_o$ .	
§ $wR(F)^2 = \{\sum [w(F_o^2 - F_c^2)]^2 / \sum [w(F_o^2)]^2\}^{1/2}$ .	

36-428 bakerite (Corkscrew Canyon) pattern with no significant differences.

EPMA analyses were obtained with a JEOL JXA 8600 instrument, with operating conditions 15 kV voltage and 20  $\mu\text{A}$  beam current. The standards used were diopside for Al and Fe and wollastonite for Ca and Si. A ZAF correction was applied. The system stability was checked three times during the working session by performing analyses of a wollastonite sample from Gavorrano, Italy.

DSC and TG curves were collected using a Netzsch STA449c instrument for datolite no. 4981 and for both no. 92735 and no. 14088 bakerite specimens. The experiments were done in nitrogen, flux 30ml/min, with a heating rate of 10  $^\circ\text{C}/\text{min}$ . The investigated temperature ranges were from 20 to 900  $^\circ\text{C}$  for the bakerite samples and from 20 to 1050  $^\circ\text{C}$  for datolite.

Infrared absorption spectra for datolite no. 4981 and bakerite samples no. 92735 and no. 14088 were recorded with a Perkin-Elmer FTIR 1725 X instrument, using the KBr method, in the range 400 to 4000  $\text{cm}^{-1}$ .

## Powder diffraction experiments

Powder diffraction data suitable for a Rietveld refinement were collected for sample no. 92735 using a conventional X-ray source, synchrotron radiation, and neutrons. For the X-ray powder diffraction experiment using a conventional source, the powder was side-loaded into a 2 mm thick flat Al holder and the data collection was performed using a Philips PW 1050/1710 instrument with a conventional Bragg-Brentano (BB) parafocusing geometry equipped with a copper tube and a secondary graphite monochromator. The data were collected in the angular range 5 to 120 $^\circ$  2 $\theta$  with steps of 0.02 $^\circ$  and 10 s/step, a divergence slit of 0.5 $^\circ$ , and a receiving slit of 0.1 mm. The refined region was 13 to 120 $^\circ$  2 $\theta$  (max  $\sin\theta/\lambda = 0.56 \text{ \AA}^{-1}$ ).

The synchrotron powder diffraction data were collected at the BM8 beamline at the European Synchrotron Radiation Source (ESRF, Grenoble, France), with an Imaging-Plate (IP) camera. The beamline geometry and the experimental setup are described in detail in Meneghini et al. (2001). The powder was mounted in a rotating 0.3 mm diameter capillary on a standard goniometric head, and the data were collected with  $\lambda = 1.0401 \text{ \AA}$  using an IP detector (Amemija 1990) mounted on a Translating Image Plate System (TIPS) (Norby 1997). The horizontal and vertical beam sizes were 1 and 0.2 mm, respectively. The wavelength was determined using the standard material LaB $_6$  in FIT2D (Hammersley 1998), which also allows for calibration of the zero-shift position of the plate, the sample-detector distance, and the tilting angle of the IP detector. The exposure time was 10 min and the diffracted data were collected at room temperature in the angular region 0 to 50 $^\circ$  2 $\theta$ . The images stored in the IP were recovered using a Fuji BAS2000 scanner through a He-Ne laser stimulation and the extracted powder patterns with a step scan of 0.02 $^\circ$  2 $\theta$  were reduced using FIT2D (Hammersley 1998).

The refined region was 7.5 to 45 $^\circ$  2 $\theta$  (max  $\sin\theta/\lambda = 0.368 \text{ \AA}^{-1}$ ).

The neutron powder diffraction experiments were performed at the Institut Laue Langevin (ILL, Grenoble, France). Because the natural sample contains about 20% B $^{10}$ , a strong neutron absorber (3835 barn at 1.6  $\text{\AA}$ ), and B $^{11} \leftrightarrow$  B $^{10}$  exchange was not possible, the absorption of B $^{10}$  had to be minimized at the expense of the counting statistics by mounting the powder in a 0.5 mm thick double walled container. The mounting procedure was performed in a glove box under a stream of nitrogen.

The room-temperature data were collected using the high-resolution two-axis diffractometer at the D1A station (Hewat and Bailey 1976). The instrument is equipped with an anisotropically squashed Ge monochromator, a beam with a high takeoff angle of 123 $^\circ$  giving high resolution at large angles, and a bank of 25 high-efficiency collimators and counters. The scan of the diffracted data suitable for a Rietveld refinement was accomplished in 48 hours. Data were collected in the angular region 0 to 160 $^\circ$  2 $\theta$ . The wavelength (1.909708  $\text{\AA}$ ) was determined by refining the standard material Cr $_2$ O $_3$  NIST 674a in GSAS (Larson and Von Dreele 1994). The refined region was 20 to 158 $^\circ$  2 $\theta$  (max  $\sin\theta/\lambda = 0.514 \text{ \AA}^{-1}$ ).

The low temperature data were collected using the high-resolution two-axis diffractometer at the D2B station (Hewat 1986). The instrument is characterized by a high take-off angle (135 $^\circ$ ) for the monochromator (Ge 335), which has a relatively large mosaic spread of 20' to compensate for the corresponding intensity loss. It is 300 mm high, focusing vertically onto about 50 mm; this large incident vertical divergence is matched by 200 mm high detectors and collimators. A complete diffraction pattern is obtained after about 100 steps of 0.025 $^\circ$  2 $\theta$ , since the 64 detectors are spaced at 2.5 $^\circ$  intervals. The set of repeated scans was accomplished in 24 hours. Data were collected at 10 K using a cryostat and the angular region was 0 to 160 $^\circ$  2 $\theta$ . The wavelength (1.59400  $\text{\AA}$ ) was determined by refining the standard material Cr $_2$ O $_3$  NIST 674a. The refined region was 14 to 147 $^\circ$  2 $\theta$  (max  $\sin\theta/\lambda = 0.601 \text{ \AA}^{-1}$ ).

## Rietveld refinements

The powder patterns for bakerite no. 92735 were refined using the GSAS software (Larson and Von Dreele 1994). For the X-ray powder diffraction data, the background profile was fitted with a Chebyshev polynomial function with nine coefficients. The diffraction peak profiles were modeled using a pseudo-Voigt function with one Gaussian and two Lorentzian coefficients. The starting atomic coordinates were taken from the datolite structure model (Foit et al. 1973) and refined in the space group  $P2_1/c$ . The refinement of the scale factor, cell parameters, background, and profile coefficients rapidly converged to a  $R(F^2)$  index of about 12% indicating that the bakerite structure is indeed close to that of datolite. In fact, the starting assumption of the proposed model was that bakerite is actually datolite with some 25% B  $\leftrightarrow$  Si substitution at the tetrahedral sites and with an extra hydrogen atom compensating for the charge misfit. The atomic coordinates, the population of Si and B in the tetrahedra, and the isotropic thermal parameters were refined with the aid of soft constraints on the tetrahedral bond lengths, which were imposed and used as additional observations in the earlier stages of the refinement and progressively reduced to zero. Tentative locations of the hydrogen atoms and water molecules as possible additional atomic species were performed with the aid of difference Fourier maps, difference Fourier peak search routines in GSAS, and geometrical considerations.

For the synchrotron powder diffraction data, the background profile was fitted with a Chebyshev polynomial function with 18 coefficients in order to correctly fit the bump in the pattern due to the scattering of the glass capillary. The diffraction peak profiles were modeled using a pseudo-Voigt function with one Gaussian and two Lorentzian coefficients. The refinement strategy was the same as described above for the conventional X-ray data.

For both the RT and the LT neutron data, necessary for the location of hydrogen atoms, the background profile was fitted with a Chebyshev polynomial function with six coefficients. The diffraction peak profiles were modeled using a pseudo-Voigt function with three Gaussian broadening coefficients and an asymmetry contribution. Again, the refinement strategy was the same as described above.

A further refinement was performed with GSAS using all the collected data (conventional X-rays, synchrotron, and neutron) inserted in the experimental file as separate histograms and using the same background and profile functions that were calculated in the separate experimental files. The same refinement strategy was used with the starting atomic coordinates taken from the datolite structure model (Foit et al. 1973). In addition, Fourier difference maps were generated using GSAS for both X-rays and neutrons and superimposed as constant density surfaces on a 3D image of the structure using the GSAS routine for producing 3D Fourier surfaces in VRML format which can be viewed with an external VRML viewer. The peaks that appeared only in the neutron map were examined as potential hydrogen sites.

## RESULTS AND DISCUSSION

The structure analysis for bakerite no. 45837 yielded a structure virtually identical in detail to that reported by Foit et al. (1973) for datolite. The atomic coordinates and equivalent

isotropic displacement parameters are reported in Table 2.

Murdoch (1962) did not report a chemical analysis for the bakerite crystals from Tick Canyon. EMPA analyses performed on Tick Canyon bakerite samples no. 45837 and no. MS1531D

**TABLE 2.** Final refined coordinates, occupancies, and isotropic displacement parameters for datolite (bakerite no. 45837) and bakerite no. 92735 (all data correspond to the latter unless noted)

Site	Single-crystal data for no. 45837*	Conventional X-ray data	Synchrotron data	Neutron data (RT)	Neutron data (LT)	Combined refinement†
Ca						
X	0.9916(1)	0.9914(4)	0.9918(5)	0.9936(10)	0.9958(13)	0.99295(28)
Y	0.1066(1)	0.10838(20)	0.10663(27)	0.1082(8)	0.1103(9)	0.10749(14)
Z	0.3357(1)	0.33369(15)	0.33305(19)	0.3315(5)	0.3326(7)	0.33320(10)
Occ.	1.0‡	1.0‡	1.0‡	1.0‡	1.0‡	1.0‡
$U_{iso}$	0.012(1)	0.026(1)	0.013(1)	0.0054(1)	0.012(1)	0.0129(4)
T1						
X	0.4692(2)	0.4738(6)	0.4793(9)	0.4761(12)	0.4768(12)	0.4754(5)
Y	0.2657(1)	0.26347(35)	0.2630(5)	0.2578(11)	0.2534(10)	0.26337(28)
Z	0.0846(1)	0.08664(32)	0.0881(5)	0.0896(9)	0.0857(7)	0.08782(24)
Occ.	1.0‡	0.75§ Si; 0.25§ B	0.75§ Si; 0.25§ B	0.75§ Si; 0.25§ B	0.75§ Si; 0.25§ B	0.75§ Si; 0.25§ B
$U_{iso}$	0.011(1)	0.025(1)	0.013(1)	0.014(2)	0.008(1)	0.0114(6)
T2						
X	0.5692(7)	0.5629(9)	0.5593(15)	0.5684(9)	0.5691(9)	0.5623(7)
Y	0.4107(5)	0.41243(69)	0.4086(10)	0.4063(11)	0.4074(9)	0.41009(59)
Z	0.3417(4)	0.33705(57)	0.3395(8)	0.3423(5)	0.3426(5)	0.33929(42)
Occ.	1.0‡	1.0‡	1.0‡	1.0‡	1.0‡	1.0‡
$U_{iso}$	0.010(1)	0.028(2)	0.021(1)	0.012(1)	0.010(1)	0.014(1)
O1						
X	0.2430(5)	0.2604(9)	0.2592(10)	0.2616(9)	0.2614(11)	0.2566(5)
Y	0.4011(3)	0.4081(6)	0.4013(8)	0.4013(8)	0.4036(9)	0.4032(4)
Z	0.0374(2)	0.0389(5)	0.0346(5)	0.0375(6)	0.0412(6)	0.03594(28)
Occ.	1.0‡	1.0‡	1.0‡	1.0‡	1.0‡	1.0‡
$U_{iso}$	0.013(1)	0.020(1)	0.011(1)	0.015(1)	0.014(1)	0.011(1)
O2						
X	0.6707(4)	0.6604(9)	0.6733(13)	0.6681(12)	0.6759(13)	0.6685(6)
Y	0.3006(3)	0.3046(5)	0.3050(8)	0.2999(6)	0.3032(8)	0.3032(4)
Z	0.4581(2)	0.4559(4)	0.4598(6)	0.4611(5)	0.4632(6)	0.45842(31)
Occ.	1.0‡	1.0‡	1.0‡	1.0‡	1.0‡	1.0‡
$U_{iso}$	0.011(1)	0.027(2)	0.011(1)	0.009(1)	0.014(2)	0.009(1)
O3						
X	0.6755(4)	0.6850(8)	0.6854(11)	0.6775(11)	0.6762(12)	0.6854(6)
Y	0.3335(3)	0.3265(6)	0.3267(8)	0.3320(6)	0.3259(8)	0.3277(4)
Z	0.2107(2)	0.2104(4)	0.2108(6)	0.2103(5)	0.2126(5)	0.21010(31)
Occ.	1.0‡	1.0‡	1.0‡	1.0‡	1.0‡	1.0‡
$U_{iso}$	0.012(1)	0.022(1)	0.010(2)	0.011(1)	0.015(2)	0.008(1)
O4						
X	0.3148(4)	0.3226(7)	0.3135(11)	0.3166(10)	0.3146(11)	0.3146(5)
Y	0.0877(3)	0.0935(5)	0.0901(8)	0.0868(8)	0.0872(8)	0.0909(4)
Z	0.1462(2)	0.1454(4)	0.1454(5)	0.1445(5)	0.1439(6)	0.14570(28)
Occ.	1.0‡	1.0‡	1.0‡	1.0‡	1.0‡	1.0‡
$U_{iso}$	0.011(1)	0.021(1)	0.019(1)	0.008(1)	0.0091(1)	0.012(1)
O5						
X	0.2587(5)	0.2582(7)	0.2540(11)	0.2595(10)	0.2581(10)	0.2557(5)
Y	0.4130(3)	0.4115(9)	0.4066(12)	0.4087(9)	0.4081(9)	0.4065(6)
Z	0.3356(3)	0.3368(5)	0.3402(5)	0.3392(5)	0.3397(5)	0.33656(29)
Occ.	1.0‡	1.0‡	1.0‡	1.0‡	1.0‡	1.0‡
$U_{iso}$	0.012(1)	0.026(1)	0.011(1)	0.012(1)	0.008(1)	0.016(1)
H1						
X	0.234(9)	-	-	0.1995(20)	0.1943(21)	0.1877(26)
Y	0.455(5)	-	-	0.4668(14)	0.4595(13)	0.4614(17)
Z	0.401(4)	-	-	0.4328(11)	0.4301(10)	0.4290(11)
Occ.	1.0‡	-	-	1.0‡	1.0‡	1.0‡
$U_{iso}$	0.020(12)	-	-	0.044(3)#	0.026(2)#	0.031(4)#
H2						
X	-	-	-	0.3994(81)	0.4142(67)	0.4265(87)
Y	-	-	-	0.4663(54)	0.4826(49)	0.4772(59)
Z	-	-	-	-0.0066(51)	0.0047(47)	0.0387(55)
Occ.	-	-	-	0.25	0.25	0.25
$U_{iso}$	-	-	-	0.044(3)#	0.026(2)#	0.031(4)#

\* Bakerite no. 45837 (= datolite).

† All the reported powder diffraction data sets were used.

‡ Fixed to 1.0 since the refined value was close to unity.

§ Independently refined to Si(T) = 0.745 and B(T) = 0.255 and fixed to the reported values.

|| Value fixed according to the stoichiometry.

# Overall refined values for the H atoms (restrained to the same value for all the H atoms).

**TABLE 3.** Chemical data for the bakerite and datolite samples

	1	2	3	4	5	6	7	8	9
SiO <sub>2</sub>	28.25	27.90	28.40	28.24	28.91	29.33	27.38	35.40	36.50
B <sub>2</sub> O <sub>3</sub>	27.30	27.58	26.57	27.42	27.66	27.25*	29.54*		23.30*
CaO	35.05	35.14	34.47	35.18	35.94	33.62	34.01	34.27	34.34
MgO				0.12					
H <sub>2</sub> O	8.46	8.60	8.37	8.56	7.12	9.60†	8.93†		5.80†
R <sub>2</sub> O <sub>3</sub>	0.94	0.65	1.93	0.48	0	0.20‡	0.14‡		0.06‡
Sum	100.00	99.87	100.00	100.04	99.71				

(1) Giles (1903); (2) Kramer and Allen (1956); (3) Kramer and Allen (1956); (4) Baysal and Dylekoz (1975); (5) Kusachi et al. (1994); (6) no. 14088, mean of 12 analysis spots; (7) no. 92735, mean of 11 spots; (8) no. MS1531D, mean of 14 spots; (9) datolite no. 4981, mean of 12 spots.

\* B<sub>2</sub>O<sub>3</sub> calculated by difference.

† Water assumed as weight loss after 110 °C in thermal analyses.

‡ Al<sub>2</sub>O<sub>3</sub> content.

are given in Table 3 as are analyses of Corkscrew Canyon bakerite samples no. 14088 and no. 92735 and datolite no. 4981. Also summarized in Table 3 are chemical data for bakerite from the literature.

Bakerite compositions are chemically well separated from datolite, and the chemical variability of Si, B, and Ca in bakerite is quite limited. Major variations relate to both the water content and to the trivalent oxide amount. The R<sub>2</sub>O<sub>3</sub> content is ascribed by Kramer and Allen (1956) to the presence of impurities. Table 3 indicates that the recent chemical data reported by Kusachi et al. (1994) are free from R<sub>2</sub>O<sub>3</sub>, and have the lowest H<sub>2</sub>O content. As stated by these authors, chemical analyses were done with material "purified by hand picking separation under a binocular microscope." The Kusachi et al. (1994) data can be recalculated on the basis of O = 40 to Ca<sub>8.04</sub>B<sub>9.96</sub>Si<sub>6</sub>O<sub>30.09</sub>(OH)<sub>9.91</sub>, closely matching the ideal bakerite formula proposed by Palache et al. (1951). This points to the possibility that minor amounts of compounds such as Al(OH)<sub>3</sub> could be intimately intermixed with the massive material from the California localities analyzed by the other authors. The presence of impurities would explain the presence of the "additional" water molecule invoked in Giles' (1903) formula. This would also explain the persistence of "additional water" in TG/DTA experiments performed by Kramer and Allen (1956), Cipriani (1958), and Baysal and Dylekoz (1975).

Among the studied samples, no. 45837 and no. MS1531D single crystals from Tick Canyon are fully confirmed by the chemical data to be datolite, while the low SiO<sub>2</sub> content in the two bakerite samples no. 14088 and no. 92735 readily discriminate them from datolite. As expected, chemical data do not give any conclusive evidence on the possible presence, or absence, of an additional water molecule in bakerite.

DTA curves for bakerite were presented by Kramer and Allen (1956), Cipriani (1958), and Baysal and Dylekoz (1975). Special attention was paid by these authors to the determination of the H<sub>2</sub>O content of their samples, as the water content is the discriminating feature between the two proposed formulae for bakerite. These authors report the occurrence of endothermic peaks, without a precise temperature, in the range 400 to 600 °C. In addition, more accurate TG/DTA data given by Kusachi et al. (1994) report the presence of two endothermic peaks at 652 and 703 °C, and a broad exothermic peak at 766 °C. All of the DTA curves are shown in Figure 1. The DTA curve obtained for datolite is in fair agreement with that of Tarney et al. (1973), with a sharp strong endothermic peak due to dehydroxylation at 733 °C. The weight loss up to 110 °C was 0.21% and up to 750 °C was 5.8%, as compared to an ideal value of 5.6%. The TG and

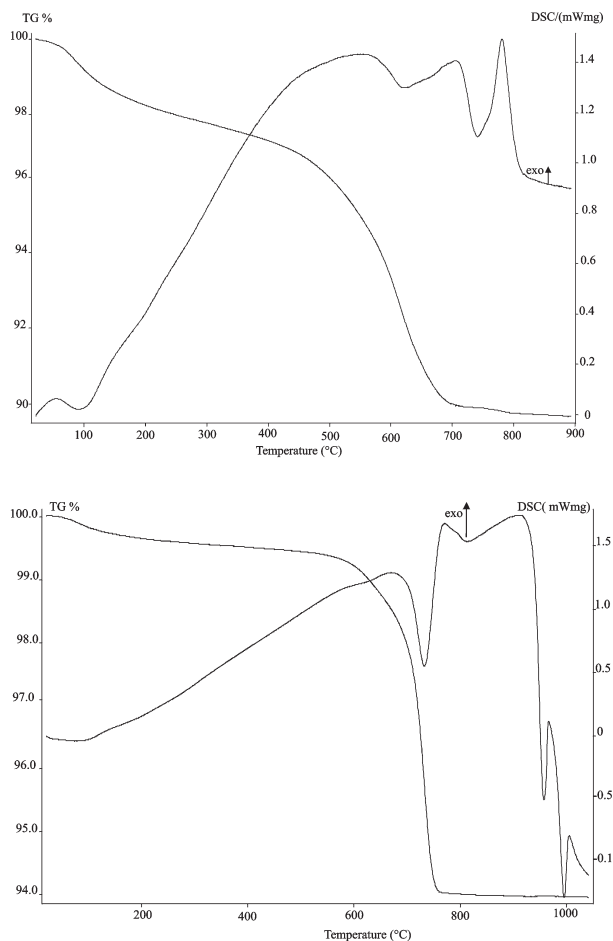


**FIGURE 1.** (a) TG/DSC curves for bakerite no. 92735. (b) TG/DSC curves for datolite no. 4981.

DSC curves obtained in the present study for the two bakerite specimens, no. 14088 and no. 92735, are markedly similar and henceforth the no. 92735 data will be assumed as representative of both samples. A broad endothermic peak is present at 625 °C, followed by a strong, sharper endothermic peak at 740 °C. Also, a distinct exothermic peak is present at 780 °C. The weight loss up to 110 °C is nearly 0.2%, and the net weight loss is 8.9% for the no. 45837 and 9.6% for the no. 14088 specimens. Comparison of our curves with those from Kusachi et al. (1994) shows that the weight loss in no. 92735 bakerite is distributed over a wider temperature range, with a first slightly sloped segment

between 200 and 450 °C, followed by a steep slope between approximately 450 and 700 °C. The peaks associated with the loss of hydroxyl groups lie at comparable temperatures in these two experiments, 652 and 703 °C in Kusachi et al. (1994), compared with 626 and 740 °C in our study. Whereas in datolite only one peak (733 °C) is associated with the loss of the hydroxyl groups, two distinct endothermic peaks are found both in our data and in those reported by Kusachi et al. (1994). These two distinct endothermic peaks for bakerite in the range 600 to 750 °C can be related to a two-step loss of hydroxyl groups.

Infrared data for bakerite from Fuka were presented by Kusachi et al. (1994), who commented on the presence of a strong absorption band at 3480 cm<sup>-1</sup>, due to the OH-stretching vibration, and on other bands around 1000 cm<sup>-1</sup>, ascribed to borates. The FTIR spectra for the no. 92735 and no. 14088 bakerite samples are nearly identical (see Fig. 2, which shows the spectra of no. 4981 datolite and no. 92735 bakerite only). To ascertain the presence of adsorbed water, the IR spectra were collected after heating the powder at 150 °C for 30 min, but no significant change was observed, thereby excluding any influence of adsorbed water on our IR spectra. Several bands are found in the region near 1500 cm<sup>-1</sup>, which is typical of borates. In both datolite and bakerite there is a strong absorption band at 3489 cm<sup>-1</sup> due to the OH-stretching vibration. Moreover, bakerite exhibits an additional distinct absorption band at 3414 cm<sup>-1</sup>, not found in datolite, which is attributable to an OH-stretching vibration. This suggests, in accordance with the TG/DSC data, some difference in the OH distribution between datolite and bakerite.

The agreement indices for the final least-squares cycles of all the structure powder refinements are reported in Table 4 together with the refined cell constants and volume. Figures 3a-d show the observed, calculated, and difference patterns. The final refined atom parameters, site occupancies, and atomic displacement parameters are reported in Table 2, together with the values obtained from the single crystal refinement of no. 45837. Table 5 reports the refined interatomic distances and angles.

Because neither the conventional X-ray data nor the synchrotron data refinements were capable of revealing the hydrogen

atom positions, neutron data collections were mandatory and indeed were fully successful. There are many examples in the literature of successful combined neutron and X-ray powder diffraction studies for accurate structure refinements or structure solutions for even more complex structures such as zeolites (Vitale et al. 1995; Harris and Tremayne 1996; Campbell et al. 2001; Lee et al. 2001). Both hydrogen atoms H1 and H2 were located even though the population of H2 was restrained to 25% according to the expected stoichiometry. Locating the proton was a challenging task since the proton population in the H2 site was close to the intrinsic resolution of the neutron powder diffraction technique. The actual limit could be identified as the location of the acid sites D3 and D5 with a population of 16%, in the neutron structure refinement of zeolite ERS-7 (Campbell et al. 2001). The average O-H distance is close to the expected value of about 1 Å for the hydrogen bond and much more accurate with respect to the value of 0.75 Å reported for the single crystal X-ray refinement of datolite (Foit et al. 1973). The refined interatomic distances are highly consistent, especially for those involving the calcium atom, which is well located even with the conventional source, given its large X-ray scattering power.

Bakerite shows two peculiar features as compared to datolite: a 25% tetrahedral substitution of B for Si at the Si-centered tetrahedra and the introduction of compensating hydrogen atoms, bonded to one of the O atoms (O1) belonging to the substituted tetrahedron. The existence of the substitution was demonstrated by direct refinement of B in the place of Si using mixed scattering factors. We started refining the T1 mixed occupancy, fixing its isotropic displacement parameter to the reasonable value of 0.01 Å<sup>2</sup>, and we obtained the following occupancies: Si(T1) = 0.745, B(T1) = 0.255, very close to the expected ratio of 1:3. In the subsequent refinement stages, we therefore assumed for the T1 site the occupancy (0.75Si + 0.25B), refining instead the displacement parameter for the T1 site. In addition, the average T-O distances reported in Figure 4 clearly show that the refined value of T-O for bakerite corresponds to an occupancy by B in T1 close to 25%. The two extremes of the linear plot in Figure 4 were respectively the mean B-O and Si-O in the two

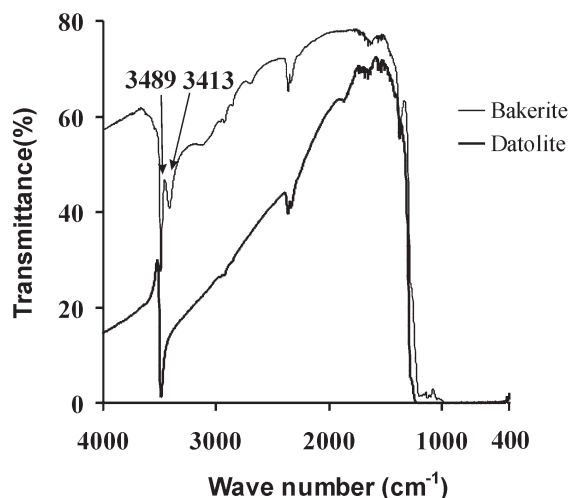
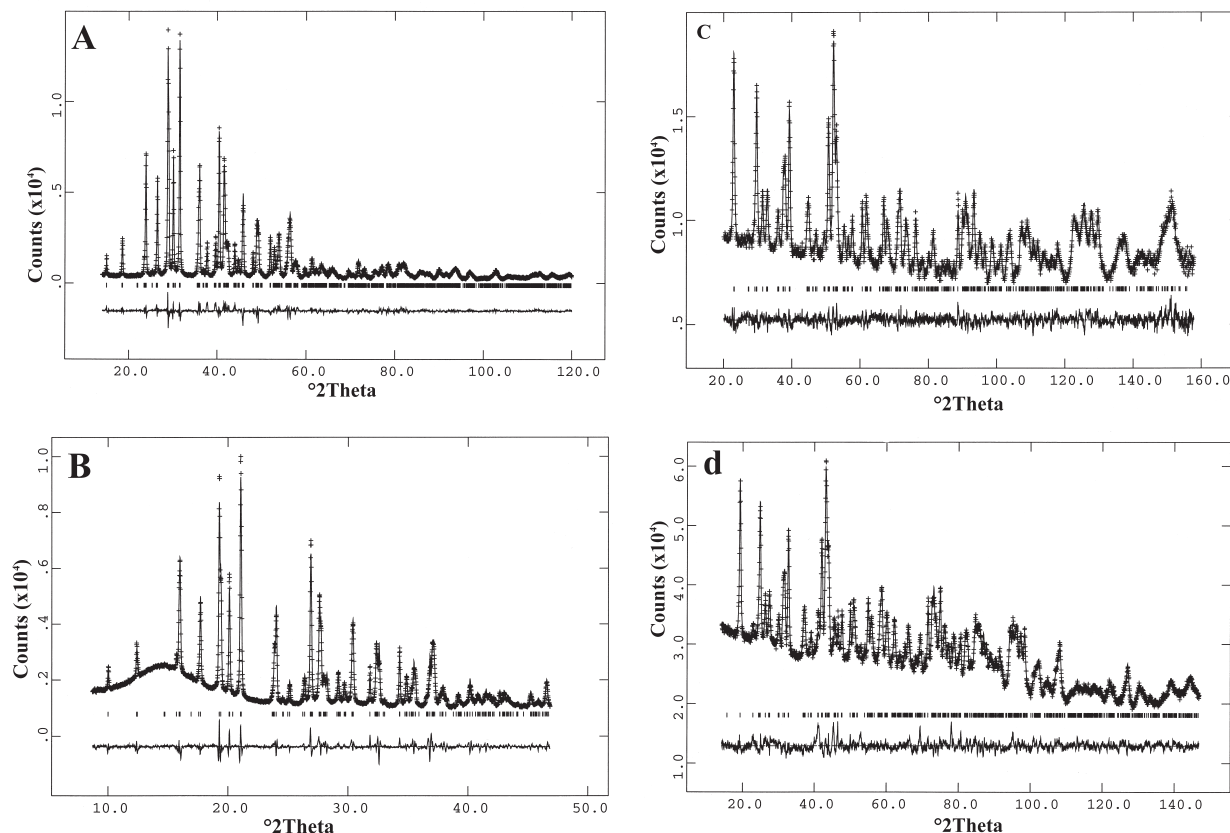


FIGURE 2. IR spectra for bakerite no. 92735 and datolite no. 4981.

TABLE 4. Rietveld refinement statistics and refined cell parameters for bakerite no. 92735

	Conventional X-ray data	Synchrotron data	Neutron data (RT)	Neutron data (LT)	Combined refinement*
<i>a</i> (Å)	4.8014(1)	4.8005(1)	4.7967(2)	4.7892(2)	4.80042(7)
<i>b</i> (Å)	7.5780(2)	7.5788(1)	7.5711(3)	7.5644(3)	7.57864(9)
<i>c</i> (Å)	9.5419(2)	9.5432(2)	9.5321(4)	9.5362(5)	9.5426(1)
$\beta$	90.434(2)	90.437(2)	90.427(4)	90.476(5)	90.435(1)
Cell volume (Å <sup>3</sup> )	347.17(1)	347.201(9)	346.16(2)	345.46(2)	347.158(5)
Observed Reflections	5310	3621	2758	2669	14277
Independent Reflections	1156	184	409	699	1156,184, 409,699
Refined Parameters	46	55	51	58	102
$R_{wp}$ (%)	8.09	4.28	2.37	2.46	4.46
$R_p$ (%)	6.35	2.96	1.94	1.83	3.09
$R(F^2)$ (%)	6.65	4.33	3.34	4.91	7.59, 4.33, 6.75, 8.21
$\chi^2$	5.8	3.64	1.7	3.69	13.1
$D_{wd}$	1.41	1.31	1.97	1.49	1.20

\* Combined refinement includes the whole set of powder diffraction data.



**FIGURE 3.** Observed (crosses), calculated (continuous line), and difference curve for the Rietveld refinements. (a) X-ray conventional data; (b) Synchrotron data; (c) Neutron room-temperature data; (d) Neutron low-temperature data. The large residual peak in Figure 3d at  $40.5^\circ 2\theta$  is a spurious peak due to the LT setting.

independent, fully occupied tetrahedra of datolite refined by Foit et al. (1973). Thus, bakerite has two independent tetrahedra  $\text{Si}_{10.75}\text{B}_{0.25}\text{O}_{3.75}(\text{OH})_{0.25}$  and  $\text{BO}_3(\text{OH})$ . As with datolite (Foit et al. 1973), the Si-rich tetrahedra are distorted with the T-O1 distance markedly shorter than the others, because O1 is the only non-shared O atom. The effect of relaxation of T-O1 due to the O1-H2 bridging is not observed here, probably because the population of H2 is only 25%. The two hydrogen atoms are bonded to the O1 and O5 atoms, respectively. Like in datolite, H1 is located near the outer surface of the tetrahedral sheet (Fig. 5a) whereas H2 is located within the tetrahedral layer (Figs. 5a and 5b) between two adjacent O1 atoms, about  $3.3 \text{ \AA}$  away from the calcium atoms. Noting that  $\text{H2-H2} = 0.87 \text{ \AA}$ , an unsuccessful attempt was made to refine H2 at the special position  $(0.5, 0.5, 0.0)$  on the inversion center with a population of 50%; moreover the long O1-H2 distance ( $1.41 \text{ \AA}$ ) obtained with H2 at the special position confirms that the best configuration is that with H2 split at the general position.

The calcium atom is located at the center of a distorted tetragonal antiprism consisting of four O atoms (O2, O3  $\times 2$ , O4), two hydroxyl groups (O5  $\times 2$ ), and two partially (25%) hydroxylated O atoms (O1  $\times 2$ ).

The identification of the hydrogen atoms, together with a close scrutiny of O...O distances shorter than  $3.1 \text{ \AA}$  between anions not belonging to the same polyhedron, allowed us to

describe a net of hydrogen bonds that contributes to the stabilization of the bakerite structure. These last distances are reported in Table 6, together with the bond-valence balance. The  $\Sigma_v$  row shows the sums of bond strengths calculated following Brese and O'Keeffe (1991), whereas in the  $\Sigma'_v$  row these sums are corrected for hydrogen bond contributions, evaluated according to Ferraris and Ivaldi (1988). The balance can be considered satisfactory. It is worth noting the O1...O1 bond ( $2.848 \text{ \AA}$ ), between adjacent O1 atoms, suggesting a possible coupled ordering of B and OH at the T1 tetrahedra, with one half of the T1 tetrahedra having the hypothetical population ( $\text{Si}_{10.5}\text{B}_{0.5}\text{O}_{3.5}\text{OH}_{0.5}$ ), the other half of the T1 tetrahedra being "pure" ( $\text{SiO}_4$ ) groups.

To further investigate the possibility of ordering, trial refinements in the lower symmetry space groups  $P2_1$  and  $Pc$  were attempted. Starting from the refined coordinates in the  $P2_1/c$  space group, models were constructed for both the  $P2_1$  and  $Pc$  space groups. Refinements in each of these space groups were attempted using both combined X-ray and neutron data and low temperature neutron diffraction data only. Soft constraints on Si-O and O-H bonds were imposed, with high statistical weights in the early stages of the refinement. The weights were gradually released during the refinement, but it was not possible to release them completely. In fact, examination of the Si-O distances in the various stages showed that they changed towards meaningless, physically unrealistic values, as the statistical weights were

**TABLE 5.** Refined interatomic distances and angles for datolite\* and bakerite no. 92735

Atoms	Datolite*	Conventional X-ray data	Synchrotron data	Neutron data (RT)	Neutron data (LT)	Combined refinement
Ca-O1	2.276(2)	2.294(5)	2.343(6)	2.352(8)	2.331(9)	2.3271(32)
Ca-O1	2.280(2)	2.341(5)	2.306(5)	2.340(7)	2.354(7)	2.3053(26)
Ca-O2	2.4538(2)	2.475(5)	2.468(7)	2.469(9)	2.461(11)	2.466(4)
Ca-O3	2.607(2)	2.501(4)	2.506(6)	2.545(7)	2.507(8)	2.5137(29)
Ca-O3	2.658(2)	2.676(4)	2.662(6)	2.652(8)	2.701(9)	2.6570(29)
Ca-O4	2.420(2)	2.411(4)	2.377(6)	2.376(7)	2.377(8)	2.3756(30)
Ca-O5	2.672(2)	2.630(6)	2.599(9)	2.609(8)	2.579(9)	2.594(4)
Ca-O5	2.518(2)	2.506(6)	2.529(7)	2.525(8)	2.547(8)	2.518(4)
Mean Ca-O	2.486	2.479	2.473	2.483	2.482	2.469
T1-O1	1.570(2)	1.566(4)	1.571(5)	1.574(9)	1.590(7)	1.5691(28)
T1-O2	1.648(2)	1.6256(34)	1.628(5)	1.599(9)	1.574(7)	1.6297(27)
T1-O3	1.651(2)	1.6227(31)	1.602(5)	1.598(8)	1.630(7)	1.6119(25)
T1-O4	1.661(2)	1.5830(33)	1.629(5)	1.594(9)	1.581(7)	1.6172(28)
Mean T1-O	1.633	1.599	1.607	1.591	1.593	1.6069
O1-T1-O2	113.95(8)	111.23(32)	110.7(5)	109.1(4)	113.0(5)	110.68(1)
O1-T1-O3	115.26(8)	114.19(28)	116.5(6)	112.0(6)	109.4(8)	115.94(2)
O1-T1-O4	108.69(8)	111.82(28)	108.4(5)	110.5(5)	110.0(6)	109.47(2)
O2-T1-O3	106.74(8)	107.86(24)	107.0(4)	107.3(3)	106.7(4)	106.61(1)
O2-T1-O4	106.15(8)	105.69(26)	106.3(6)	108.0(6)	110.2(8)	106.51(2)
O3-T1-O4	105.34(8)	105.51(31)	107.3(3)	109.6(7)	107.1(8)	107.14(2)
Mean O-T1-O	109.36	109.38	109.36	109.4	109.4	109.39
T2-O2	1.475(3)	1.471(4)	1.492(6)	1.468(7)	1.481(6)	1.4830(34)
T2-O3	1.486(3)	1.497(4)	1.507(6)	1.478(7)	1.481(6)	1.5067(33)
T2-O4	1.464(3)	1.487(4)	1.511(6)	1.479(9)	1.475(7)	1.4988(35)
T2-O5	1.496(3)	1.463(4)	1.466(6)	1.482(7)	1.489(6)	1.4719(31)
Mean T2-O	1.480	1.479	1.494	1.476	1.481	1.4901
O2-T2-O3	107.9(2)	104.9(4)	105.2(5)	109.4(7)	107.9(8)	105.44(2)
O2-T2-O4	109.5(2)	108.1(4)	105.3(6)	108.7(9)	107.1(3)	107.04(3)
O2-T2-O5	111.1(2)	108.1(5)	110.5(8)	109.9(9)	110.8(2)	109.96(3)
O3-T2-O4	106.9(1)	110.2(4)	106.7(9)	106.8(7)	108.8(9)	107.46(2)
O3-T2-O5	109.48(2)	113.2(4)	114.0(8)	110.3(3)	109.8(7)	112.11(4)
O4-T2-O5	111.9(2)	111.9(4)	114.3(9)	111.2(4)	112.0(7)	114.31(5)
Mean O-T2-O	109.5	109.4	109.33	109.3	109.4	109.390
H1-O5	0.75(5)†	-	-	1.037(13)	0.996(11)	1.031(9)
H2-O1	-	-	-	0.93(4)	1.008(17)	0.995(11)

\* Single-crystal refinement data (Foit et al. 1973).

† In the original paper it is H-O(5).

**TABLE 6A.** Bond valence (v.u.) calculations and hydrogen bonds for bakerite

	O1	O2	O3	O4	O5	$\Sigma a_v$
Ca	0.378	0.260	0.228	0.331	0.184	2.163
	0.401		0.155		0.226	
T1	1.017	0.863	0.905	0.893		3.677
T2		0.739	0.693	0.708	0.761	2.901
H1					0.749	1.000
H2	0.25					0.25
$\Sigma c_v$	2.046	1.862	1.981	1.931		
$\Sigma c_v$	2.046	1.987	1.981	2.057	1.920	
O1-O1	2.848					
H1...O4	2.188	0.126				
H1...O2	2.191	0.125				

**TABLE 6B.** Simulation of charge balance on O1 (see Figs. 7a and 7b), assuming coupled full occupancy by (OH)<sup>-</sup> for the O1 site and by B<sup>3+</sup> for the T1 site and taking into account hydrogen bonds contribution

	O1	O1'	O1''
Ca	0.378	0.378	0.378
	0.401	0.401	0.401
T1 = B	0.81		
T1 = Si		1.08	1.08
H2	0.83	0.17	
$\Sigma c_v$	2.42	2.03	1.86

decreased. This is most probably due to the pseudosymmetries relating couples of atoms, independent in both  $P2_1$  and  $Pc$  space groups, which were symmetry equivalent (by the inversion center) in the space group  $P2_1/c$ .

Notwithstanding the slight decrease in the agreement factors observed refining both in  $P2_1$  and in  $Pc$ , a physically meaning-

ful change in atomic positions and distances was not detected. Therefore, although the hypothesis of long-range order of silicon and boron at the T1 site, and correspondingly the ordering of H2 hydrogen atoms, cannot be excluded, we have assumed the reasonable crystal chemical model refined in the  $P2_1/c$  space group.

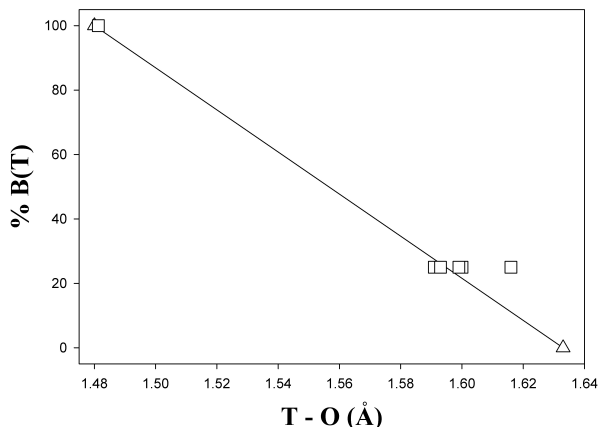


**FIGURE 4.** The mean T1-O distances for bakerite, obtained with the different refinements (5 values; Table 5), are denoted as open squares; also the grand total of the mean T2-O distances (1.484 Å) is denoted as open square. The mean value for T1-O and T2-O reported by Foigt et al. 1973 for datolite are shown as triangles.

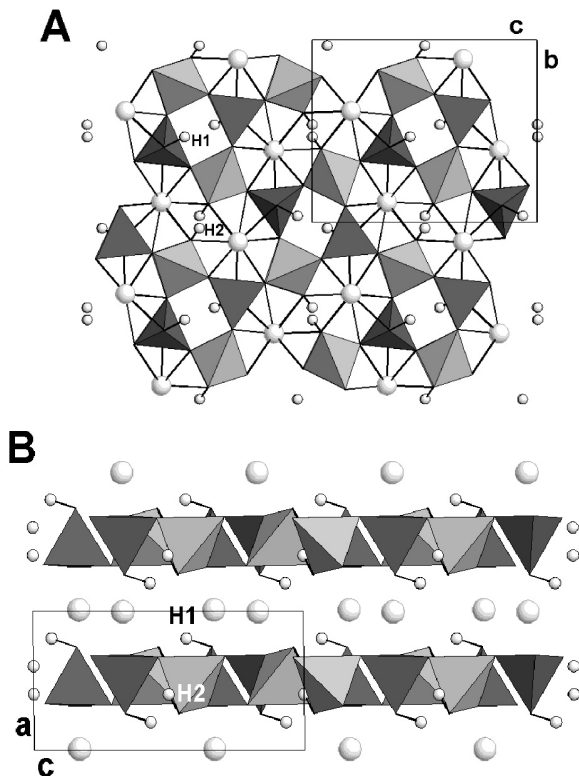


**FIGURE 5.** (A) The crystal structure of bakerite projected onto the (100) plane. The T1 tetrahedral set is indicated by the lighter gray shade, the T2 tetrahedral set by the darker one. (B) The crystal structure of bakerite viewed along [010]. As in datolite, the H1 hydrogen atom is located on the edge of the tetrahedral sheet, whereas the H2 hydrogen lies inside the tetrahedral sheet.

The random substitution of one B atom for Si at one of the four T1 sites in bakerite determines a B-polyhedral cluster, which is not described in the list of possible borate clusters (Burns et al. 1995; Hawthorne 1983; Hawthorne et al. 1996). Here a

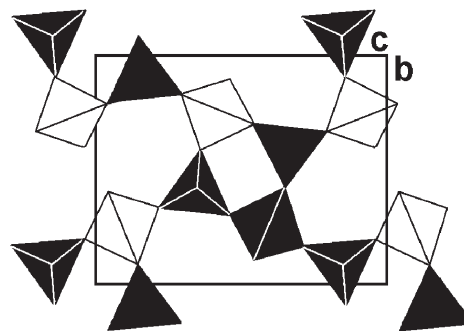


**FIGURE 6.** The polyhedral cluster formed by four  $B\phi_4$  tetrahedra in bakerite: the cluster is built up by three T2 tetrahedra and one T1 tetrahedron, drawn black to indicate it is occupied by B.

cluster of four  $B\phi_4$  tetrahedra is formed with the B-substituted tetrahedron sharing three out of four corners with the other tetrahedra (Fig. 6).

No borate rings are formed and according to the specific algebraic descriptors (Burns et al. 1995) such a configuration should be referred as  $4\Box:4\Box$ . This polyhedral cluster is not observed in nature and is not even mentioned in the frequency of occurrence of selected clusters as FFBs in borate minerals after Burns et al. (1995). There is a close similarity to the B-polyhedral cluster exhibited by uralborite,  $Ca_2[B_4O_4(OH)_8]$  (Simonov et al. 1977), which shows a decorated  $\langle 3\Box \rangle \Box$  ring, the only difference being the two outer tetrahedra forming the 3-membered ring that are not connected in the bakerite cluster.  $CaB_2O_3(OH)_2$ , with a datolite structure exhibiting a sheet of 4-membered and 8-membered B-centered tetrahedra in the b-c plane ( $\langle 8\Box \rangle = \langle 4\Box \rangle$ ) has never been found among the natural borate structures. In fact, only johachidolite (Moore and Araki 1972),  $Ca_2Al_2[B_6O_{14}]$  with an FBB consisting of a 6-membered ring of tetrahedra that shares an edge with a 4-membered ring of tetrahedra ( $\langle 6\Box \rangle = \langle 4\Box \rangle$ ) has some weak similarity with the B-cluster connectivity of the hypothesized  $CaB_2O_3(OH)_2$ .

#### SI $\leftrightarrow$ B SUBSTITUTION IN BAKERITE

One might expect the  $Si + O^{2-} \leftrightarrow B + (OH)^-$  substitution to commonly occur in datolite, at least between the Si/B ratios 1:1 (datolite) to 5:3 (bakerite). Literature chemical data for datolite (Deer et al. 1963; Grew 1996) shows instead a close stoichiometric composition for datolite from worldwide occurrences. The composition of bakerite (Table 3) is also quite constant, apart from those elements ascribed (see preceding discussion) to the presence of minor impurities. These considerations suggest that it is worth looking for a possible explanation for the peculiar stoichiometry of bakerite, based on the local charge balance consequent to the  $Si + O^{2-} \leftrightarrow B + (OH)^-$  coupled substitution.

Consider (Figs. 7a and 7b) the columns of T1 tetrahedra, running along [100], and facing each other. The data presented in Table 6 (bond-valence balance) indicate a good balance for O1 for the average situation (random distribution of 3Si and 1B at the T1 tetrahedra). However, when the T1 tetrahedron is actually occupied by B and OH is placed in O1 to restore the charge balance, a heavy "supersaturation" results for O1, as reported in Table 6b. The values of Table 6b are taken from those given in our Table 5, recalculated for  $T2 \equiv B$  and considering that H2 now

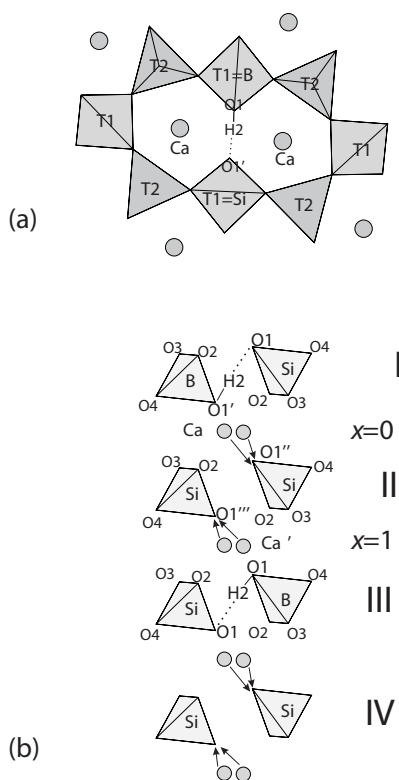


**FIGURE 7.** (a) An eight-membered ring in the tetrahedral sheet of bakerite (see also Fig. 5a), projected onto (100), with the T1 “double columns” hosting the  $\text{Si} + \text{O}^{2-} \leftrightarrow \text{B} + (\text{OH})^-$  coupled substitution. Ca cations are shown as gray shaded circles. (b) The boron and hydroxyl entrance in the T1 “double columns,” shown running along [100]. The movement of the Ca cations to restore the local charge balance is shown by the arrows.

has full occupancy and distributes its bond valence between O1 and O1' [0.87 and 0.13 v.u. were calculated according to Ferraris and Ivaldi (1988) for the hydrogen bond  $\text{O} \cdots \text{O}$  2.848 Å].

To remove the large unbalance on O1 the Ca cations at  $x \approx 0$ , which form strong bonds (2.305 and 2.327 Å) with O1, move away from the plane toward the other pair of T1 tetrahedra. The O1" atom cannot be involved in hydrogen bonding (neither as the O1–H2 nor as H2···O1), because Ca cations now give a “bond” contribution higher than 0.78 v.u. (shorter bond distances). Therefore, both tetrahedra at level II are occupied by Si, as indicated in Figure 7b: both O1" and O1"' are pure  $\text{O}^{2-}$  anions (H2 absent); consequently also, Ca' moves from the plane toward the tetrahedral pair in II to compensate for undersaturation. This allows or stimulates the simultaneous entry of B and OH in the adjacent level III, with the consequences already described for level I.

Therefore, in all the double columns of T1 tetrahedra, we have an ordered distribution of boron and silicon tetrahedra, with a strong hydrogen bond O1–H2···O1 (2.848 Å), and the correct B:Si ratio (1:3). The position of the “starting” B tetrahedron may be different in the different double columns, resulting in an apparently random distribution of silicon and boron at T1. This ordering places an upper limit on the B:Si ratio, which is realized when B cations enter in all the “double columns,” and

which corresponds to the 5:3 value actually found in all the bakerite specimens.

The substitution scheme just discussed explains why the highest B:Si ratio in datolite-type structures is 5:3. It would be interesting to determine why no intermediate composition has been found between datolite,  $\text{Ca}_8\text{B}_8\text{Si}_8\text{O}_{32}(\text{OH})_8$  and bakerite,  $\text{Ca}_8\text{B}_{10}\text{Si}_6\text{O}_{30}(\text{OH})_{10}$ . No simple crystal-chemical explanation may be presently offered.

Although in a strict sense bakerite could be considered to be a boron hydroxylated datolite and, therefore, discredited as a mineral species, two considerations argue for the retention of bakerite as a distinct species: (1) Bakerite samples from different localities and distinct geological environments are quite similar in composition, particularly with respect to their Si and B contents. (2) Bakerites constantly show the highest allowed B:Si ratio, 5:3. There appears to be no evidence of substitution of B for Si in datolite or, in other words, there is no evidence for any solid solution between datolite,  $\text{Ca}_4\text{B}_4\text{Si}_4\text{O}_{16}(\text{OH})_8$ , and bakerite,  $\text{Ca}_4\text{B}_5\text{Si}_3\text{O}_{15}(\text{OH})_5$ . Molecular dynamics simulations and experimental studies in the  $\text{CaO}-\text{B}_2\text{O}_3-\text{SiO}_2-\text{H}_2\text{O}$  system might provide an explanation for the “mixing gap” between datolite and bakerite.

#### ACKNOWLEDGMENTS

C. A. Francis is acknowledged for providing a type specimen of bakerite from the collection of the Harvard Mineralogical Museum. Single-crystal structure data collection was performed in the X-ray Crystallography Laboratory of the Department of Chemistry and Biochemistry, University of California, Los Angeles. S. Khan is acknowledged for his technical assistance. M. Lezzerini of the Earth Science Department of the University of Pisa is kindly acknowledged for his assistance in obtaining the TG/DSC spectra. For the neutron experiments, E. Suard is kindly acknowledged as the local contact with the D1A and D2B beamlines at ILL (exp. Nr. 5-21-866). For the synchrotron experiments, C. Meneghini is kindly acknowledged as the local contact at the BM8 beamline at ESRF (exp. Nr. 08-02-267).

#### REFERENCES CITED

- Amemija, Y. (1990) X-ray area detector based on photostimulable phosphor. *Synchrotron Radiation News*, 3, 21–26.
- Baysal, O. and Dilekoz, E. (1975) A study of bakerite. *Bulletin of the Mineral Research and Exploration Institute of Turkey*, 84, 90–96.
- Brese, N.E. and O'Keeffe, M. (1991) Bond-valence parameters for solids. *Acta Crystallographica*, B47, 192–197.
- Burns, P.C., Grice, J.D., and Hawthorne, F.C. (1995) Borate minerals I. Polyhedral clusters and fundamental building blocks. *Canadian Mineralogist*, 33, 1131–1151.
- Campbell, B.J., Cheetham, A.K., Vogt, T., Carluccio, L., Parker, W.O., Flego, C., and Millini, R. (2001) The determination of Brønsted acid sites in zeolite ERS-7 by X-ray and neutron powder diffraction. *Journal of Physical Chemistry*, B 105, 1947–1955.
- Cipriani, C. (1958) Ricerche sulla disidratazione di alcuni borati naturali. *Atti Società Toscana Scienze Naturali Serie A*, 65, 284–322.
- Deer, W.A., Howie, R.A., and Zussman, J. (1963) *Rock Forming Minerals. Vol. I: Ortho and Ring Silicates*. Longmans, London.
- Ferraris, G. and Ivaldi, G. (1988) Bond valence vs. bond length in  $\text{O} \cdots \text{O}$  hydrogen bonds. *Acta Crystallographica*, B44, 341–344.
- Foit, F.F., Phillips, M.W., and Gibbs, G.V. (1973) A refinement of the crystal structure of datolite,  $\text{CaBSiO}_4(\text{OH})$ . *American Mineralogist*, 58, 909–914.
- Giles, W.B. (1903) Bakerite (a new borosilicate of calcium) and howlite from California. *Mineralogical Magazine*, 13, 353–355.
- Grew, E.S. and Anovitz, L.M. (1996) Boron: Mineralogy, petrology and geochemistry, vol. 33. *Reviews in Mineralogy, Mineralogical Society of America*, Washington, D.C.
- Hammersley, A. (1998) FIT2D V10.3 Reference Manual V4.0—ESRF98HA01T
- Harris, K.D.M. and Tremayne, M. (1996) Crystal structure determination from powder diffraction data. *Chemistry of Materials*, 8, 2554–2570
- Hawthorne, F.C. (1983) Graphical enumeration of polyhedral clusters. *Acta Crystallographica*, A39, 724–736.
- Hawthorne, F.C., Burns, P.C., and Grice, J.D. (1996) The crystal chemistry of boron. In Grew, E.S. and Anovitz, L.M., Eds., *Boron: Mineralogy, petrology and geochemistry*, 33, 41–115. *Reviews in Mineralogy, Mineralogical Society*

- of America, Washington, D.C.
- Hewat, A.W. (1986) D2B, a new high resolution powder diffractometer at ILL. *Material Science Forum*, 9, 69–79.
- Hewat, A.W. and Bailey, I. (1976) D1A, a high resolution neutron powder diffractometer with a bank of mylar collimators. *Nuclear Instrumentation Methods*, 137, 463–71.
- Kramer, H. and Allen, R.D. (1956) A restudy of bakerite, priceite, and veatchite. *American Mineralogist*, 41, 689–700.
- Kusachi, I. (1994) Chemical composition of bakerite from Fuka, Okayama Prefecture, Japan. *Mineralogical Journal*, 17, 111–117.
- Larson, A.C. and Von Dreele, R.B. (1994) Los Alamos National Laboratory Report LAUR 86–748.
- Lee, Y., Reisner, B.A., Hanson, J.C., Jones, G.A., Parise, J.B., Corbin, D.R., Toby, B.H., Freitag, A., Larese, J.Z., and Kahlenberg, V. (2001) New insight into cation relocations within the pores of zeolite rho: In situ synchrotron X-ray and neutron powder diffraction studies of Pb- and Cd-exchanged rho. *Journal of Physical Chemistry B*, 105, 7188–7199.
- Meneghini, C., Artioli, G., Balerna, A., Gualtieri, A.F., Norby, P., and Mobilio, S. (2001) Multipurpose imaging-plate camera for in-situ powder XRD at the GILDA beamline. *Journal of Synchrotron Radiation*, 8, 1162–1166.
- Moore, P.B. and Araki, T. (1972) Johachidolite,  $\text{Ca Al} [\text{B}_3\text{O}_7]$ , a borate with very dense atomic structure. *Nature*, 240, 63–65.
- Murdoch, J. (1962) Bakerite crystals. *American Mineralogist*, 47, 919–923.
- Norby, P. (1997) Synchrotron powder diffraction using imaging plates: crystal structure determination and Rietveld refinement. *Journal of Applied Crystallography*, 30, 21–30.
- Palache, C., Berman, H., and Frondel, C. (1951) *Dana's System of Mineralogy*, 7th edition, Vol. II, 363.
- Palenzona, A. (1985) Bakerite: first discovery in Italy. *Rivista Mineralogica Italiana*, 2, 67–68.
- Pemberton, H.E. (1971) Type locality for bakerite. *American Mineralogist*, 56, 1109–1110.
- Sabina, A.P. (1978) Some new mineral occurrences in Canada. *Geological Survey of Canada, Paper 78-1A*, 253–258.
- Simonov, M.A., Egorov-Tismenko, Y.K., and Belov, N.V. (1977) Accurate crystal structure of uralborite,  $\text{Ca}_2[\text{B}_4\text{O}_4(\text{OH})_8]$ . *Soviet Physics Doklady*, 22, 277–279.
- Tarney, J., Nicol, A.W., and Marriner, G.F. (1973) The thermal transformation of datolite,  $\text{CaBSiO}_4(\text{OH})$ , to boron-melilite. *Mineralogical Magazine*, 39, 158–175.
- Vitale, G., Bull, L.M., Morris, R.E., Cheetham, A.K., Toby, B.H., Coe, C.G., and MacDougall, J.E. (1995) Combined neutron and X-ray powder diffraction study of zeolite Ca L5X and a  $^2\text{H}$  NMR study of its complex with benzene. *Journal of Physical Chemistry*, 99, 16087–16092.

MANUSCRIPT RECEIVED JUNE 24, 2003

MANUSCRIPT ACCEPTED NOVEMBER 12, 2003

MANUSCRIPT HANDLED BY BRYAN CHAKOUMAKOS